



A universal approximation of grain size from images of noncohesive sediment

D. Buscombe,^{1,2} D. M. Rubin,³ and J. A. Warrick³

Received 3 August 2009; revised 10 December 2009; accepted 21 January 2010; published 10 June 2010.

[1] The two-dimensional spectral decomposition of an image of sediment provides a direct statistical estimate, grid-by-number style, of the mean of all intermediate axes of all single particles within the image. We develop and test this new method which, unlike existing techniques, requires neither image processing algorithms for detection and measurement of individual grains, nor calibration. The only information required of the operator is the spatial resolution of the image. The method is tested with images of bed sediment from nine different sedimentary environments (five beaches, three rivers, and one continental shelf), across the range 0.1 mm to 150 mm, taken in air and underwater. Each population was photographed using a different camera and lighting conditions. We term it a “universal approximation” because it has produced accurate estimates for all populations we have tested it with, without calibration. We use three approaches (theory, computational experiments, and physical experiments) to both understand and explore the sensitivities and limits of this new method. Based on 443 samples, the root-mean-squared (RMS) error between size estimates from the new method and known mean grain size (obtained from point counts on the image) was found to be $\pm\approx 16\%$, with a 95% probability of estimates within $\pm 31\%$ of the true mean grain size (measured in a linear scale). The RMS error reduces to $\approx 11\%$, with a 95% probability of estimates within $\pm 20\%$ of the true mean grain size if point counts from a few images are used to correct bias for a specific population of sediment images. It thus appears it is transferable between sedimentary populations with different grain size, but factors such as particle shape and packing may introduce bias which may need to be calibrated for. For the first time, an attempt has been made to mathematically relate the spatial distribution of pixel intensity within the image of sediment to the grain size.

Citation: Buscombe, D., D. M. Rubin, and J. A. Warrick (2010), A universal approximation of grain size from images of noncohesive sediment, *J. Geophys. Res.*, 115, F02015, doi:10.1029/2009JF001477.

1. Introduction

[2] Grain size is of fundamental importance, governing the mechanical, electrical and fluid dynamic properties of sediment. The surface texture of a noncohesive, un lithified sediment bed, as sensed by a photographic device, is the two-dimensional projection of its three-dimensional structure. Using photographs to quantify grain size (and other properties) of ancient or modern sediment beds, in an automated fashion, is of considerable interest because it is relatively cheap and rapid, and thus can allow much greater coverage and resolution of grain size measurements compared to traditional methods [Rubin, 2004]. This is because measurements from digital images are orders of magnitude

faster than physical measurements such as sieving and settling [Barnard *et al.*, 2007]. In addition, measurements are nonintrusive and sample only those grains that are exposed to the flow and are thus subject to transport or winnowing.

[3] Images of natural sediment beds are complex, typically composed of at least several hundred individual grains all varying in area, form, angularity, color, etc. In addition, grains overlap and this casts shadows across the surface which are irregular in size and spatially random in color. Existing methods of automated grain size estimation from images rely on calibration [e.g., Rubin, 2004; Carbonneau *et al.*, 2004, 2005; Verdú *et al.*, 2005; Buscombe *et al.*, 2008], or on advanced sequences of image processing to isolate and measure each individual grain [e.g., Graham *et al.*, 2005], or both, which are often sediment population specific. In this contribution, we describe a new method for estimating mean grain size from an image which overcomes both these disadvantages.

[4] The problem of accurate and automated grain size estimation from an image of natural sediment can be

¹United States Geological Survey, and Institute of Marine Studies, University of California, Santa Cruz, California, USA.

²Now at School of Marine Science and Engineering, University of Plymouth, Plymouth, UK.

³U.S. Geological Survey, Santa Cruz, California, USA.

approached in two fundamentally different ways. The first, what we term a “geometrical” approach, is essentially deterministic in the sense that it attempts to measure the outlines of each grain (or portion of grain) within the image, and in turn assign a measurement to it. In this way, a grain size distribution may be built up, from which population statistics such as the mean may be calculated.

[5] In essence, this approach attempts to use sophisticated sequences of image processing algorithms to filter and detect grain boundaries in an automated fashion, to mimic what a person may achieve by manually digitizing grain boundaries by eye. The problem is complicated in the absence of a “background” image intensity against which to isolate (threshold) the pixel boundaries of individual particles, but has been successfully overcome on dry coarse gravel river beds, usually, but not exclusively, supported in a sand or fine gravel matrix [Sime and Ferguson, 2003; Graham et al., 2005]. It remains, however, difficult to design a “universal” algorithm which is truly transferable between different sediment populations, and which is equally applicable across the range of noncohesive sediment sizes, because each population creates different optical artefacts caused by the reflection of ambient and flash light (grain-shading issues), and/or bed and grain structure (e.g., imbrication, or intragranular marks and scratches). Procedural bias which causes oversegmentation or undersegmentation of particles within the image (which results in finer or coarser particles, respectively, than in reality) will hinder the geometrical approach until algorithms are designed which use some “artificial intelligence” to detect or deterministically model, and thus account for or remove the influence of, the length scale of such optical artefacts. In other words, even a perfect geometrical (edge detection) approach would also need to recognize partially concealed grains and exclude them from analysis, or alternatively include a statistical algorithm to estimate the full size of the partially concealed grains.

[6] The second approach to the problem is what we term “statistical,” which treat pixel intensity variations in an image as realizations of a stochastic process. The approach is substantially different from other forms of particle size analysis, both physical methods such as sieving/callipers and geometrical image analysis as described above, because instead of (deterministically) trying to detect and measure each grain, the goal of a statistical approach is to characterize the mean grain size (or other feature of interest). Thus these methods directly receive information from, but do not directly measure, the distribution of sizes. Rather, this approach uses mathematical/statistical tools on the digital image of sediment treated as a two-dimensional matrix of discrete numbers, to describe the geometry of the features (i.e., grains). A statistical approach thus avoids the difficulties associated with perfectly detecting the boundaries of every grain in an image, regardless of sediment type and the grain size fraction. Further, a statistical approach can operate at finer scales (down to the theoretical limit of 1 pixel per grain) compared to geometrical approaches [Carbonneau, 2005], which in general require several pixels per grain (e.g., at least 23 for the technique of Graham et al. [2005]). Another advantage of such an approach is that it, potentially, allows the mean grain size (or other property of interest) within an

image to be expressed as a mathematical abstraction of the spatial arrangement of image intensity.

[7] One such statistical approach consists of deriving image statistics using spatial (morphological) operations to decompose the image. For example, Buscombe and Masselink [2009] progressively degraded images of sediment and used a measure of the loss of detail to calculate the image’s fractal dimension. It was found that this dimension was linearly related to sediment size. A similar approach was used by Lian et al. [2004] on thin sections of sandstone to derive the physical dimensions of pore spaces. Such an approach requires considerable computational time, and is sensitive to the choice of structure function shape and increments in their size, in order to overcome the influence of optical “noise” which, by definition, occurs at wavelengths smaller and greater than the typical range of grain diameters. Another statistical type of approach might use gradients in pixel intensity across sediment images to characterize the typical length scale of grains. It has thus far been used on images of sediment for orientation analyses [e.g., Tovey and Hounslow, 1995], but not yet for physical estimates of mean grain size. Such an application might too be hampered by a subjective choice of window size to negate (spatially filter) the influence of optical noise. Such a choice becomes more difficult the more mixed (poorly sorted) the grain size distribution within the image.

[8] It is more desirable to have a method in which no prior estimate of feature size needs to be made through tunable parameters such as search window size, i.e., one which uses only the information in the image to derive a measure sensitive to the length scale of grains. Such methods follow from Rubin [2004], who showed that for images of natural sediments with different mean grain size, and taken with the same camera, the spatial autocorrelation coefficient at a given lag is a function of the mean grain size. The spatial autocorrelation profiles (correlograms) from a set of calibration images (of known sediment size) can be used to give highly accurate estimates of mean grain size from a given sample image by solving a simple least squares problem. This approach has been shown to be highly accurate for close-up photographs of sand and gravel [Rubin et al., 2007; Barnard et al., 2007; Buscombe and Masselink, 2009; Warrick et al., 2009] and similar techniques have been shown to work well for larger-scale, coarser-resolution imagery from aerial platforms [e.g., Carbonneau et al., 2004, 2005; Carbonneau, 2005]. The approach is designed to include and nullify specific sources of variability in sample images by including them in the calibration. Such variability comes from two sources: the camera system (lens, spatial distortions and lighting), and the nonrandom aspects to the structure of the sediment bed (for example imbrication, and correlations of grain size with grain shape and color). However, a consensus is yet to be reached with regard to the sensitivity of results to calibration design and content, so a universal algorithm (i.e., one that does not need calibration) is desirable. For example, pressing questions include how many grain size fractions the catalogue should contain, to what pixel lag, and what degree of overlap is acceptable in the calibration curves.

[9] Buscombe and Masselink [2009] showed that the spatial autocorrelation algorithm was one of several suitable

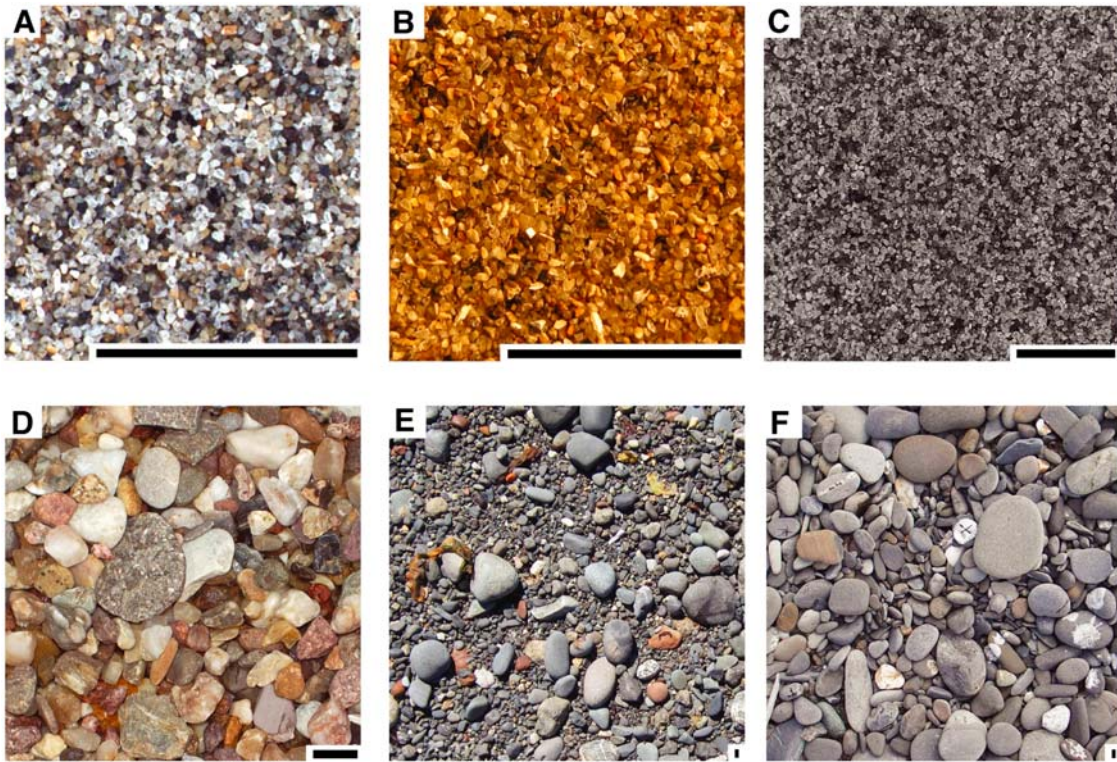


Figure 1. Images of sediment. The black bar in each image represents 1 mm. (a) River sand (with macro lens, illuminated by a LED ring; dimensions 2448×2050 pixels; resolution 0.018 mm/pixel). (b) Inner shelf sand (dried, handheld digital camera in macro mode, taken with a handheld Pentax Optio WP, illuminated by table lamp; dimensions 3264×2448 pixels; resolution 0.0076 mm/pixel). (c) Beach sand (wireless camera, illuminated by LEDs; dimensions 1300×1160 pixels; resolution 0.0068 mm/pixel). (d) Beach gravel (50 cm from bed inside a black box, illuminated by camera's flash; dimensions 2048×1536 pixels; resolution 0.04 mm/pixel). (e) River gravel/cobbles (illuminated by natural sunlight; dimensions 1700×1500 pixels; resolution 0.46 mm/pixel). (f) Beach gravel/cobbles (illuminated by natural sunlight; dimensions 800×1600 pixels; resolution 0.46 mm/pixel).

techniques which could be used within the calibration framework of *Rubin* [2004], including variograms and spectra. *Buscombe* [2008], drawing from work utilizing variance spectra of sedimentary rock thin sections to describe their stochastic geometry [e.g., *Preston and Davis*, 1976; *Lin*, 1982], described a technique using the two-dimensional correlogram of an image in order to estimate the major and minor grain diameters. Furthermore, it was suggested that the diameter of some contour between 0 and 1 of the two-dimensional surface of autocorrelation from an image of sediment should be related to the mean grain size, which in turn suggested that an uncalibrated estimate of mean grain size directly from the image might be possible.

[10] Here, we propose such a method to estimate mean grain size from an image that requires neither calibration nor image segmentation procedures. The method is tested with 443 images of natural sediment beds composed of mixed grain sizes, with mean grain sizes spanning 3 orders of magnitude, from 0.1 to 150 mm, from nine different sedimentary populations, each with a different camera and lighting system. We use three approaches (theory, computational experiments, and physical experiments) to both

explain these results and explore the limits at which uncalibrated estimates begin to fail.

2. Method

2.1. Theory

[11] To be useable in our method of grain size analysis, an image of sediment (e.g., Figure 1) should contain only noncohesive un lithified clastic material, where the entire image is composed of touching grains at rest. The lighting, provided by a natural or artificial source, should be such that the illuminated surface is discretized by the camera. The image should have a reasonably high contrast, meaning that the pixel values, in 8-bit intensity (greyscale) form, are highest (i.e., lighter) on tops and flanks of individual grains, lowest (i.e., darker) in the pores between grains and that there is a noticeable gradient in pixel intensity with distance across the grain/pore from highest to lowest value. The above is also conditional on the image having an adequate spatial resolution (which can usually be discerned by eye, but which we also address experimentally in section 5.2). If all visible particles in an image were well illuminated, the entire image would be represented by sediment. In reality,

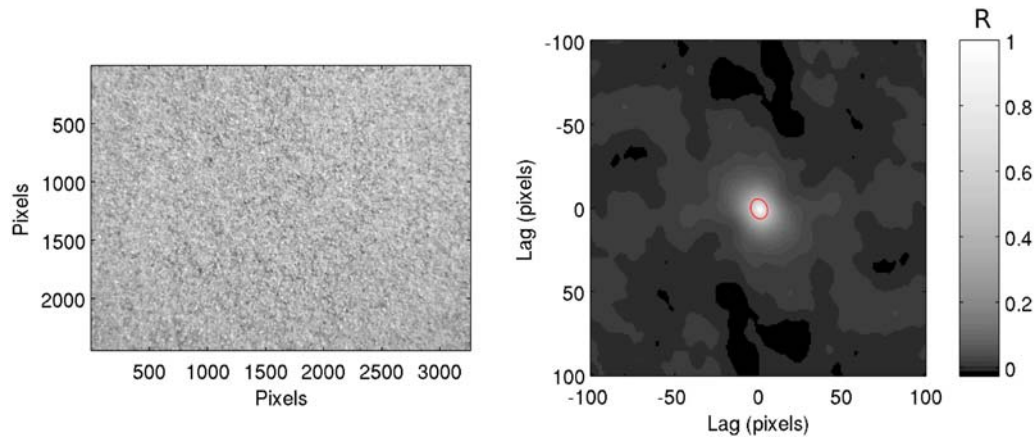


Figure 2. (left) Image of sediment and (right) the center 200×200 pixel section of its autocorrelation surface. The contour $R = 0.5$ is highlighted by red line. The image (resolution 0.0076 mm/pixel) is of shelf sand, taken with an off-the-shelf point-and-shoot digital camera with macro capabilities, illuminated using a desk lamp. The contour of $R = 0.5$ (Figure 2, right) is elliptical, oriented along the left-right diagonal. The major and minor axes of this diagonal are 6.02 and 4.83 pixels, respectively, corresponding to grain diameters of 0.286 and 0.229 mm.

images will have dark regions between grains caused by insufficient lighting. More pronounced under ambient solar illumination, geometrical methods are especially sensitive to the effects of the intergranular shadows [Graham *et al.*, 2005]. For the purposes of this paper, we define these dark regions in images of sediment as “pores,” which should not be confused with the more common definition of sediment porosity, even though these quantities may be related.

[12] Griffiths [1961] suggested that a sedimentary bed is a function of 5 fundamental properties: size, shape, orientation, packing and mineralogy. Photographs of sediment capture all of these properties (Figure 1), and if the grains therein are homogenous and isotropic (i.e., sections through, or subareas of, the image have similar statistical properties) the two-dimensional variance spectrum, hereafter simply “spectrum,” should contain information of all Griffiths’ elements except those aspects of mineralogy related to grain color [Preston and Davis, 1976].

[13] Although autocorrelation has been used for grain size analysis [Rubin, 2004], its original development was in one dimension using stepwise (spatial) calculations of correlation. Here we follow Buscombe [2008] by presenting an extension of these one-dimensional autocorrelation techniques into a two-dimensional form in the frequency domain rather than the spatial domain. Buscombe [2008] suggested the use of the two-dimensional autocorrelation function (here denoted R , Figure 2) since the transform normalizes magnitudes of spectral density, thus different images are comparable. The spectrum of an image simultaneously maps its entire contents into frequency space and thus information can be used to quantify the dominant wavelength of features therein. This property has been used to characterize the texture and geometry of sedimentary rocks [Preston and Davis, 1976; Lin, 1982; Torabi *et al.*, 2008] as well as unlithified sediment surfaces [Buscombe, 2008]. In this contribution, we find a generalized solution to the problem, thus removing the dependency on calibration. The new approach can be carried out with correlograms derived in the

1D or 2D approaches, but the 2D approach is recommended for the reasons stated above, and what follows concerns only 2D correlogram estimation.

[14] The spectrum of a demeaned image, denoted f' , is the Fourier transform of the autocovariance function, which in turn is the dimensional form of the autocorrelation function (R). The spectrum of pixel intensity in an image may be expressed as the Fourier dual:

$$f'(x) = \int_{-\infty}^{\infty} e^{ikx} \psi(k) dk \quad (1)$$

$$\psi(k) = \frac{1}{2\pi} \int_{-\infty}^{\infty} e^{ikx} f'(x) dx \quad (2)$$

where x is the spatial (lag) index, i is the imaginary unit, and e is the base of the natural logarithm. Here k is the wave number, the spatial analog of frequency (in other words, the number of times the function f' has the same phase per unit space). Before applying the fast Fourier transform, each pixel is multiplied by $-1^{(x+y)}$ to center it, and the mean subtracted from each pixel to eliminate harmonics. The two-dimensional autocorrelation function $R(x)$, normalized by its total power, is found by computing the inverse Fourier transform of its spectrum $\psi(k)$ [Preston and Davis, 1976]:

$$\psi(k) = \frac{1}{2\pi} \int_R e^{ikx} R(x) dx \quad (3)$$

[15] Fara and Scheidegger [1961] showed that, in a simplified one-dimensional case, the power spectral density expressed in such a form invariant of the origin is the sum of its real and imaginary parts, and is given by $\psi(k)\psi^*(k)$ where $*$ denotes complex conjugate. Expressed as such, intervals of lengths other than 2π can be handled by scale factors, and the wavelength of both f' and $R(x)$ can be given by $\Lambda(k) = 2\pi/k$, where k has dimension length^{-1} [Fara and

Table 1. Details and RMS Errors Associated With Each of the Nine Sediment Populations Tested in This Study^a

	Site	Environment	Camera	N	% Error	% Error, No Bias	S
1a	Santa Cruz, Ca	shelf sand	u/w ^b video, m ^c	7	30.01	12.89	1.66
1b	Santa Cruz, Ca	shelf sand	p-a-s ^d , m	10	10.56	6.24	1.53
2	Slapton, UK	beach gravel	p-a-s	116	20.52	12.42	1.75
3	Unknown (aggregate)	river gravel	p-a-s	16	6.44	4.97	2.22
4	Colorado River	river sand	u/w slr ^e , m	16	18.10	6.51	1.75
5a	Pescadero, Ca	beach sand	u/w slr, m	8	8.60	4.93	1.43
5b	Pescadero, Ca	beach sand	p-a-s, m	6	9.91	3.71	1.44
6	Columbia River, Wa	beach sand	u/w slr, m	176	12.38	10.47	1.05
7	Santa Barbara, Ca	beach sand	u/w slr, m	49	16.90	15.29	1.25
8	Kachemak Bay, Al	beach cobble	p-a-s	10	13.98	10.01	5.34
9	Elwha, Wa	beach cobble	p-a-s	29	30.30	11.59	4.05

^aNote that Santa Cruz and Pescadero populations have been split into two, because two different camera/lighting systems were used for each. N, sample population (number of images, each containing a different sediment sample).

^bUnderwater.

^cMacro lens.

^dPoint-and-shoot (handheld).

^eSingle lens reflex. S, sorting coefficient (ratio of 84th and 16th percentiles; *Folk and Ward* [1957]).

Scheidegger, 1961], or 1/pixels. Thus a waveform given by e^{-ikx} will have wavelength (periodicity) $\Lambda = 2\pi/k$, and the autocorrelogram of such a function should be in antiphase at $\Lambda/2$ (half wavelength) lags; equal 0 at $\Lambda/4$ lags; and equal 0.5 at $\Lambda/(2\pi) = k$ lags. This suggests that the lag at which $R = 0.5$ is a suitable value for k . The theory should be equally valid in two-dimensional images if the grains are statistically homogenous. In other words, the first-order statistics of enough 1D sections through the image are the same, in which case the theory outlined above is equally as valid in 2D as in a collection of 1D sections.

2.2. Application to Images

[16] The authors' collective research efforts into statistical methods (section 1) for automated grain size estimation has resulted in a collection of hundreds of images of sediment for which a measurement of the mean grain size is available. All images were of natural noncohesive nonorganic sediment, either taken in situ in the field, or photographed in the laboratory. Mean size was determined by manual "point count" on the images, which is considered the benchmark against which to test results from statistical methods applied to (2D) images, rather than sieving [*Barnard et al.*, 2007; *Rubin et al.*, 2004; *Warrick et al.*, 2009]. In each digital image, a grid composed of a 100 intersections was drawn and the intermediate diameter of the grain (pore to pore) underneath each grid intersection measured (therefore a grid-by-number estimate). Note this is the intermediate projected axis which is apparent in the image, not the true (or calipered) intermediate axis. Both automated and manual techniques measure this. Counting grains at every grid intersection makes the grain selection free from operator bias. Where the grain at a grid point is not fully exposed (i.e., partially hidden by other grains), the person doing the counting moves to the first complete grain located in a specified direction. For further validation of this procedure, see *Barnard et al.* [2007].

[17] A total of 443 images were used in this study, across the size range 10^{-1} to $10^{2.2}$ mm, from nine different sedimentary populations (five beaches, three rivers, and one continental shelf; see Table 1), in situ (undisturbed), and taken both in air and underwater. Each sediment population

was photographed using a different camera and lighting. All the images used were those of a sediment bed in plan view, containing noncohesive clastic material only, and where the entire image is composed of touching grains. Both subaqueous and subaerial images are equally suited to the new measure, as long as bubbles or other features do not obscure the scene. General guidelines and hardware requirements for suitable image collection in a range of subaerial and subaqueous environments may be found in the work of *Rubin et al.* [2007], *Buscombe and Masselink* [2009], and *Warrick et al.* [2009].

[18] We used these images to experimentally verify that the optimum objective value of k is found as the lag at which the image's autocorrelation surface (R) equals 0.5, in line with the simple theory outlined above. This was achieved by computing the correlogram for each image to find lags associated with a range of coefficients of R , then substituting these values for k , and correlating the resulting grain size estimates with the true mean grain size for each image. We confirmed the lag at which $R = 0.5$ as the appropriate value for k , since this value yielded the highest correlation between observed and estimated mean grain size. Thus scaling by the image resolution r (in units of length/pixel), provides a universal measure which scales to near unity with measured mean grain size, z :

$$z = (2\pi r)/k \quad (4)$$

[19] Lag k may vary as a function of cross section through R (Figure 2) if the grains in the image have any preferred orientation. In this case the value of k (in pixels) is found as the radius of an ellipse fitted to the coordinates $[m, n]$ of the contour $R = 0.5$ (Figure 2), following the method outlined in Appendix A. The intermediate radius best agreed with true mean size for images used in this study, and the major radius is suggested only where a significant proportion of grains in an image appear smaller than they really are due to partial burial by other grains (imbrication). Thus the intermediate radius was found to correspond with the mean of intermediate (b) grain axes. Ascribing the exact physical equivalence of other measures of the ellipse, such as the mean

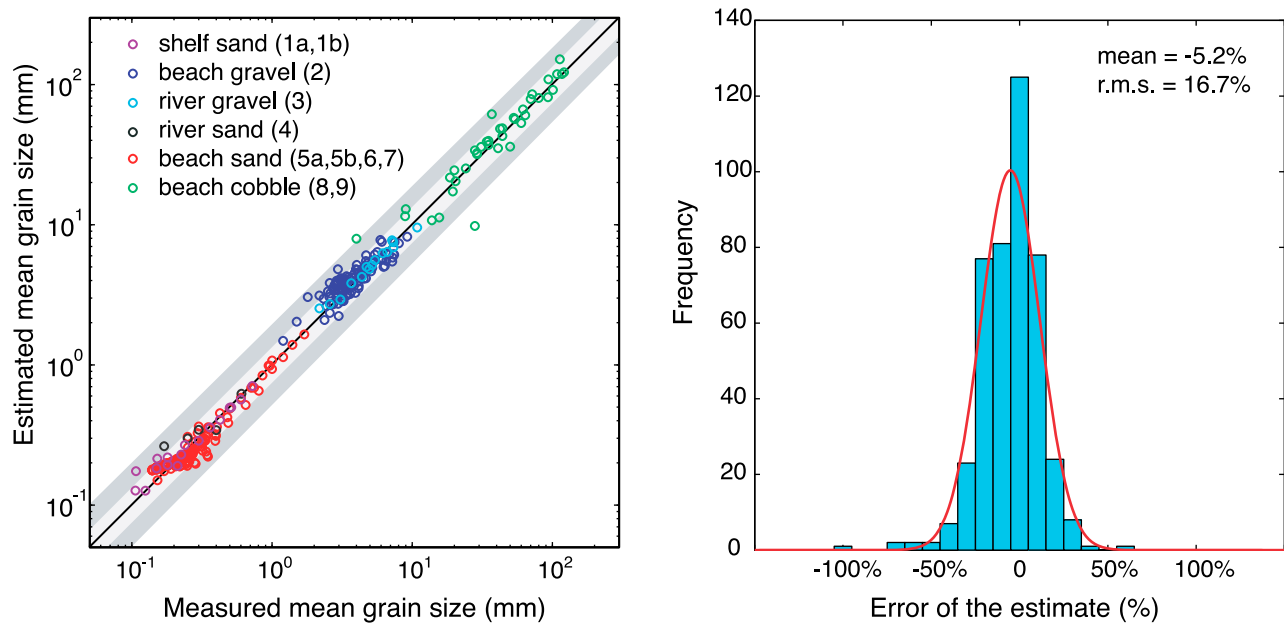


Figure 3. (left) Measured versus estimated grain size (mm), in log-log space. The lighter shaded region represents the 95% confidence interval of the results, and the darker shaded region represents a 100% discrepancy, for which only two samples exceed. Different marker colors indicate each population of sediments. Note that Santa Cruz and Pescadero populations have been split into two, because two different camera/lighting systems were used for each. Therefore, there are 11 “populations” represented in total. (right) Histogram of the percent errors for individual samples, with mean and RMS error values (in percent) for the entire sample population annotated.

radius, was not attempted here but might be useful in studies where the natural packing of grains with respect to their exposed axes is of unusual character or special concern.

[20] Figure 3 (left) shows the comparison of estimated to true mean grain size, both in millimeters, for each of the nine tested sediment populations (Table 1). Figure 3 (right) shows the histogram of individual errors is approximately normal around zero (with a mean error of -5%) which experimentally verifies our choice of 0.5 for the value of grain length scale k (we return to the value of k in section 5.1. from a more theoretical standpoint). Note that although the percentage-based errors appear to be linear, the normalization makes these values nondimensional and therefore nonlinear and roughly equivalent to a ϕ -based measurements [cf. Warrick *et al.*, 2009]. The root-mean-squared (RMS, or “irreducible”) error (which includes both systematic or procedural bias, and random error/scatter) was calculated as 16.7%. These stated errors contain uncertainties in both the measurements from the on-screen point counting procedure and the estimates using the automated technique.

[21] For a similarly sized sample (≈ 100 measurements), Rice and Church [1996] suggest that physical measurements of the clasts should result in $\sim 0.1\phi$ standard error in the estimate of the mean. Considering that the mean grain sizes of their samples were -4.1 to -5.1ϕ , this is equivalent to $\sim 2\%$ RMS error in the estimate of the mean. However, Warrick *et al.* [2009] showed that the photo count methods resulted in a 7% mean irreducible error in estimates of intermediate axis lengths. We postulate that the errors are larger because the operator carrying out point counts finds it

more difficult to identify the intermediate axes of grains than an operator with calipers in the field.

[22] The effect of the photo count error on our total analysis error should be assessed in quadrature rather than in a linear manner, owing to the likely independence of measurement and estimation errors. Our total analysis error is between $\sim 10\%$ and $\sim 17\%$, so the “unresolvable” contribution is between $\sqrt{0.1^2 - 0.07^2} = 7\%$ and $\sqrt{0.17^2 - 0.07^2} = 15\%$. Thus errors introduced by the on-screen point counts are significant, although they are secondary to the remaining errors of the analysis.

[23] For all populations there is a bias between the best linear fit between true and estimated mean size, and the 1:1 relationship (Figure 4). The slope and intercept coefficients of a linear regression can be used to correct for this systematic bias. However, reduced major axis (RMA) regression is more appropriate than standard ordinary least squares (OLS) regression when the independent variable, in this case the mean size calculated from the point counting procedure, is measured with error [Davis, 1986]. Based on the recommendation of McArdle [1988], who suggests that RMA should be used when the error rate in the independent variable exceeds one third of the error in the dependent (it does in our case: 7% versus 16%), we used RMA regression following Davis [1986].

[24] This bias-correcting procedure produces the same effect as, in a practical application of the technique outlined in this paper, carrying out manual point counts on a few “end-members” of the population, then correcting for any bias by finding the RMA best fit between the estimate based on point counts, and the estimate derived from this new

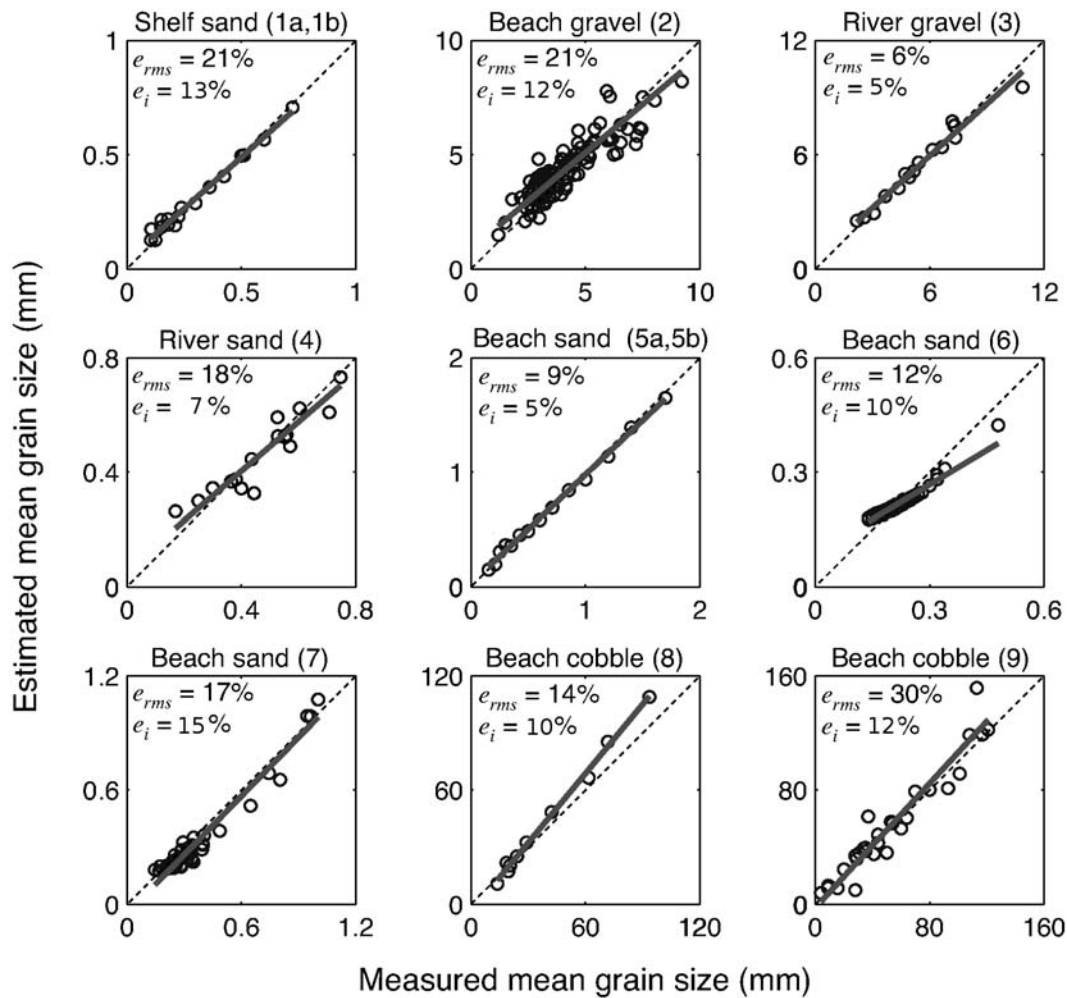


Figure 4. Results from each of the nine tested populations (in Table 1 and Figure 3), separated and in linear space (mm). The 1:1 relationship is shown by the dashed line and the reduced major axis (bias corrected) best fit as the heavy line. Individual population RMS (e_{rms}) and bias-corrected RMS (e_i) errors are noted in each subplot.

automated technique. Expressing errors relative to the RMA fit between sample measures and estimates substantially reduces the RMS error to 11% by correcting for bias. Figure 4 shows the results from each of the nine populations in linear space, with best fit lines fitted through each to show the deviation from the 1:1 relationship, and with the bias-corrected relationships and RMS errors annotated in terms of percentages. Using a cumulative probability curve (Figure 5) compiled using all 443 sample images, the new method has a 95% chance of being within 20% for bias-corrected, and 31% for noncorrected estimates, of the true mean grain size. The results for all tested sediment populations are summarized in Table 1.

[25] The errors for these uncalibrated noncorrected estimates, for sediments which vary in size over 3 orders of magnitude, are equal to or slightly higher than those reported by previous researchers working with single size fractions (either sand or gravel or cobble alone, and excluding other size fractions even when present in the image) using other similar methods designed for the same purpose. The errors for bias-corrected estimates (tantamount to “semicalibration”), however, are equal to or smaller than

errors reported for similar techniques. *Graham et al.* [2005] is currently the best geometrical technique for images of natural sediment, reporting a 13% error (log scale) in controlled lighting in the 16–90 mm particle size range [*Warrick et al.*, 2009]. Using the statistical calibrated autocorrelation technique of *Rubin* [2004], *Barnard et al.* [2007] (0.1–1.4 mm), *Buscombe and Masselink* [2009] (1–16 mm), and *Warrick et al.* [2009] (1–200 mm) reported RMS errors (in linear scales) of, respectively, $\approx 10\%$, 13% and 7–14%.

[26] We note that the range of (uncorrected) errors in Table 1 is quite large, between 6 and 30% depending on the population. It is clear that image resolution is important in minimizing errors. For example, this must in part account for the differences in errors between populations 1a (30%) and 1b (10%) since they are the same sediment population but the cameras used differ in resolution by an order of magnitude (essentially being the difference between a video camera and a high-end handheld). This is further highlighted by the fact that populations 5a and 5b have almost identical errors: they are the same sediment population taken with different cameras with almost identical resolutions. However, image resolution alone does not account for the

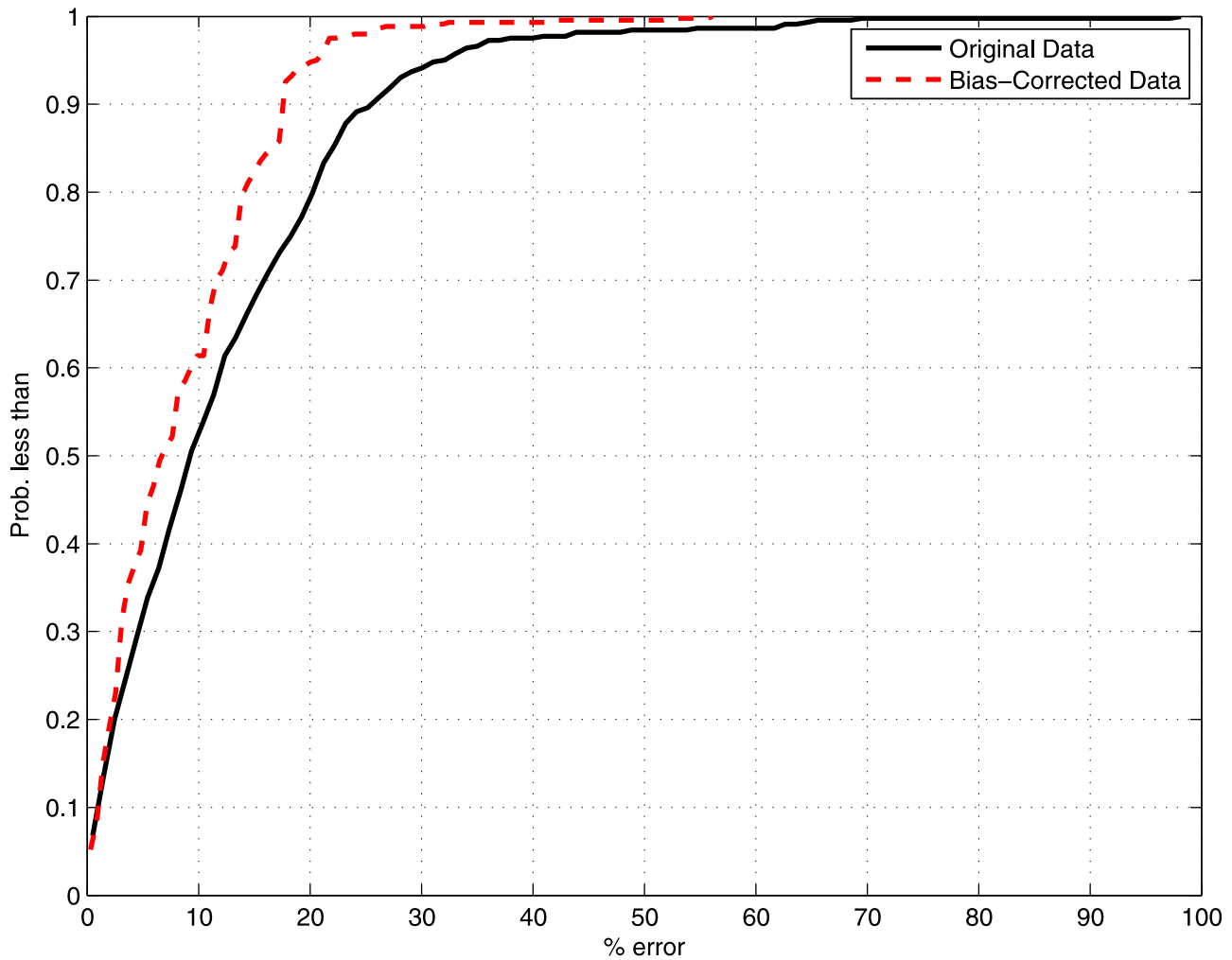


Figure 5. Cumulative probability of less than stated percent error for original (noncorrected, solid) and bias-corrected (dashed) data. The 90th and 95th percentiles for noncorrected estimates are 25.17% and 32.07% and for bias-corrected estimates 17.22% and 20.04%, respectively.

range in errors. For example, populations 8 and 9 are very different sedimentologically, and have very different errors, but were photographed with the same camera. It is likely in this case (and, interestingly, perhaps only this case) that the large errors are caused by poor sediment sorting.

3. Effects of Sample Size and Grain Shading

3.1. Computer Simulations

[27] In an image of sediment adequately resolved and composed of touching grains with no preferred shape or orientation, on a flat surface parallel to the camera (i.e., plan view), the new measure (equation (4)) quantifies the diameter of a typical grain because the contrast in shading between pixels on grains and pixels on pores is sufficiently large. In other words, on a mean grain length scale, local pixel intensity tapers from maximum at the center of a grain to minimum at the center between grains. This seems to be important to the success of the new measure and suggests that illumination with a strong directionality would have a deleterious effect. The fact that percent discrepancies are approximately equal across the size range suggests that

potentially nonoptimal shading artefacts scale with mean grain size. In order to explore this further, computer simulations of sediment beds were used to investigate the uncertainty in grain size estimates due to variable shading. Using computer simulations, it is possible to objectively and independently vary shading, and generate many hundreds of beds with which to test and verify ideas. We hypothesized that the new measure would be sensitive to aspects of grain shading which make the grains appear larger or smaller, on average, than they really are.

[28] In an image, grains are not uniformly shaded primarily because they differ in color. The length scale of this variation is determined by the mean diameter of the grains, or the mean distance between grains. It is also in part a function of lighting. In a poorly illuminated image, grains may appear smaller because light does not penetrate sufficiently into (and reflect from) the pore spaces, whereas in a well-illuminated image, the apparent diameter of the grains is maximized. We term these collective effects “intergranular shading,” a term with close connotations with the more common notion of image “contrast.” Marks, scratches and hollows on individual grains, caused by the original crystal

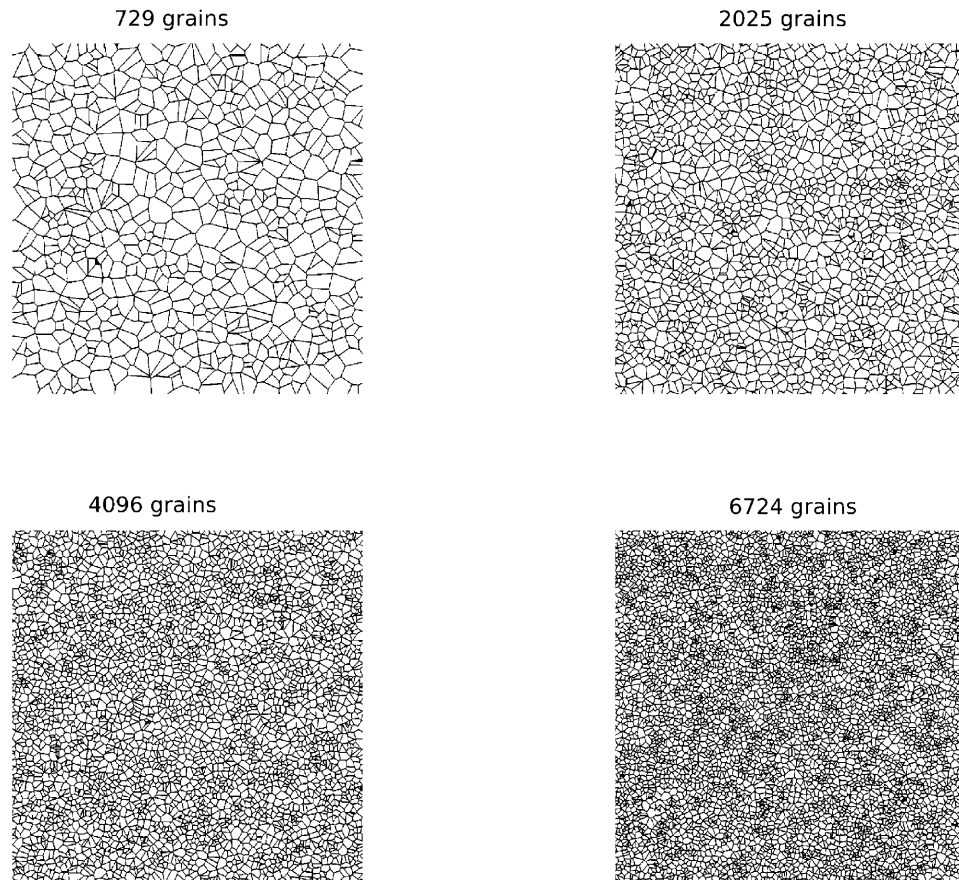


Figure 6. Poisson-Voronoi tessellations with different numbers of polygons/grains. These form the basis of the synthetic sediment beds generated to evaluate and test the contributions of shading variations to method errors.

shape and chemical/physical weathering, cause diffuse reflectance which creates small patches of darker shading at scales smaller than a grain's mean diameter. Light patches smaller than a grain's diameter may be caused by either diffuse interreflection, or specular reflectance from protruding, angular, and crystalline surfaces on grains. The collective term for the shorter-wavelength deviations from the grain shade is intragranular shading.

[29] A stochastic model was developed to create synthetic sediment beds containing grains which are random in size, shape, orientation and location. In this model, a range of particle (2D) sizes, shapes and orientations is allowed to exist, and particles of a given size, shape and orientation are randomly distributed across the image/surface. A range of particle colors can exist, which in an intensity image corresponds to several shades of grey. Collectively, this ensures that the bed is homogenous and isotropic in a statistical sense, but its random intergrain and intragrain properties can be modified independently or simultaneously.

[30] A suitable approach to the realization of random sediment bedding is a space-filling tessellation based around a random (in space) distribution of points. Consider the centroid coordinates of grains in an image. The relative position of each of these points, set V , in space is dictated by the relative size and shape of each grain it represents. For each of these points V_x the boundary enclosing all the

intermediate points lying closer to V_x than to any other point is called a Voronoi polygon (also known as a Dirichlet region or Thiessen polygon). A set of tessellating Voronoi polygons based upon a set of points randomly distributed in space, a so-called Poisson-Voronoi tessellation, bears remarkable resemblance to a natural sediment bed [Barndorff-Nielsen, 1989] (also Figure 6). In particular, Voronoi tessellations are a form of convex polygon, appropriate since natural sediment grains do not tend to have inward facing edges in planform.

[31] In a fixed area, the general form of a size distribution can be controlled by changing the number of polygons (grains), itself fixed by the number of coordinate pairs generated by a random number generator (Figure 6). Since the coordinates of the boundary of each grain are known, highly accurate estimates of the areas and axial dimensions of these polygons can be made. The ratio of grain pixels to gap pixels is controlled either using a combination of morphological operations on images of the random tessellations (we use morphological dilation using a circular structure function which expands the grains into the gaps), and/or by applying a scaling factor to each polygon. The synthetic beds have bed packing densities similar to those found in nature (between 0.6 and 0.7, or 1 minus porosity). The particle size distributions and particle packing densities generated by the model are akin to those found in natural

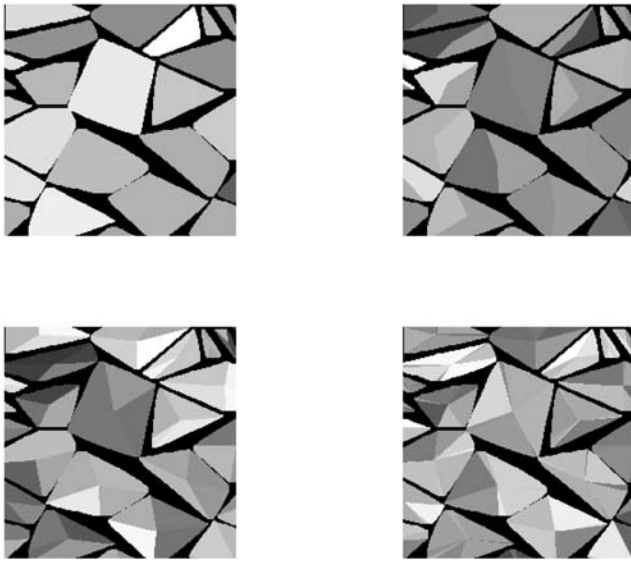


Figure 7. Examples of the same grains in the synthetic bed model with different degrees of shading (different numbers of shaded facets per grain).

sediments. It has long been established that natural particle size distributions are log-hyperbolic in form [Bader, 1970; Barndorff-Nielsen, 1977]. Note that the log-hyperbolic family of distributions includes the lognormal distribution as a limiting case [Fieller *et al.*, 1992]. In order to test the size distributions of the synthetic surfaces, we fitted the hyperbolic distribution density function directly to the observed data (measured grain diameters, rather than a mass size distribution evaluated at discrete size intervals; see Appendix B). The analysis confirmed that synthetic sediment surfaces very closely follow a log-hyperbolic distribution after a population size of about 1000 grains, and this

model fits the data better than a lognormal distribution. As a rule of thumb, therefore, images should contain at least 1000 grains (or ≥ 32 in any cross section through a square image). In images of real sediment, this is approximately the number less than which there is a high probability that the correlogram does not fall to a value of 0.5.

[32] A surface composed of Poisson-Voronoi tessellations resembles one which has been fractured into a set of smaller pieces at random locations. In such cases it has been shown that the particle area a and diameter z are related by $z \approx a^{0.5}$ [Grady, 1990], and it is important to note that the same general relationship is found in the grain area and diameter distributions of the computer-simulated sediment surfaces.

[33] The model was used to generate sets of beds where the intergrain and intragrain shading was varied independently. For each case, nine images were generated, containing between 1000 and 10000 individual grains. Intragrain shading was varied by generating four sets of nine beds containing grains each with either one, two, four, or eight shaded facets (e.g., Figure 7). In these intragrain tests, intergranular shading was held constant (black). This had the effect of progressively increasing the variability of individual particle shading.

[34] Interparticle shading was controlled by shading in the pore spaces between particles, from all black pore space, to pore space identical to that of the mean grain shade. Five sets of nine beds were generated with pore intensities zero (all black), 25, 50, 75, and 100% mean grain shade. In these intergranular shading tests, in each case the grains has just one shaded facet (i.e., the intragrain shading was held constant).

3.2. Simulation Results

[35] Figure 8 summarizes the results of the tests with variable intergranular and intragrain shading, for all 81 test synthetic beds (4×9 variable intragrain shading beds, and 5×9 variable contrast/intergranular shading

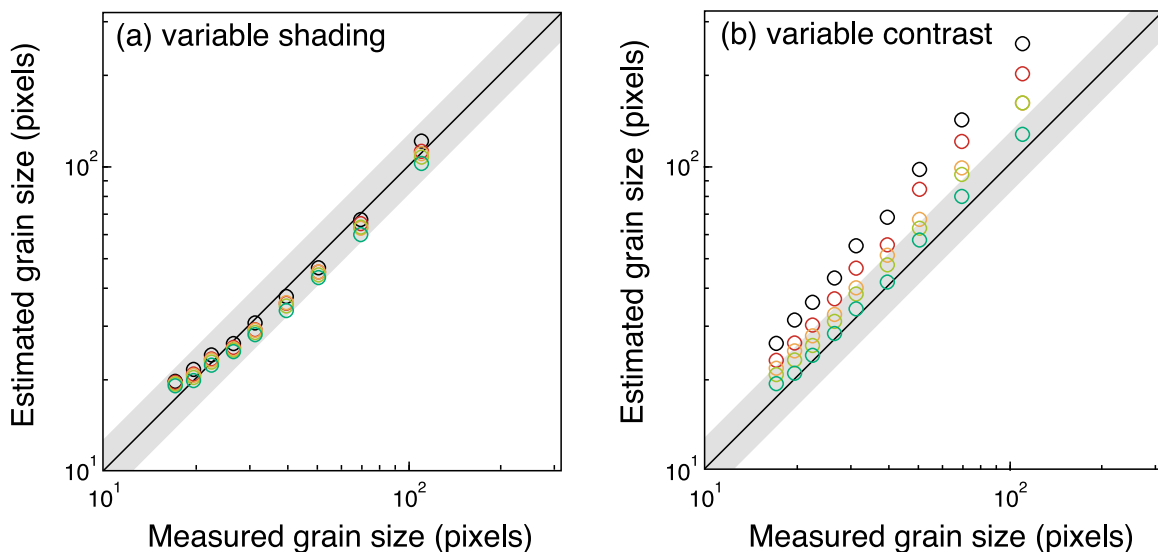


Figure 8. Effect of intergranular and intragrain shading on estimated mean grain size results. (a) The effect of variable shading (intragrain shading): four sets of grain shading variations for each of the nine sizes. (b) The effect of variable contrast (intergranular shading) on estimated mean grain size: five sets of contrast (particle-pore) variations for each of the nine sizes.

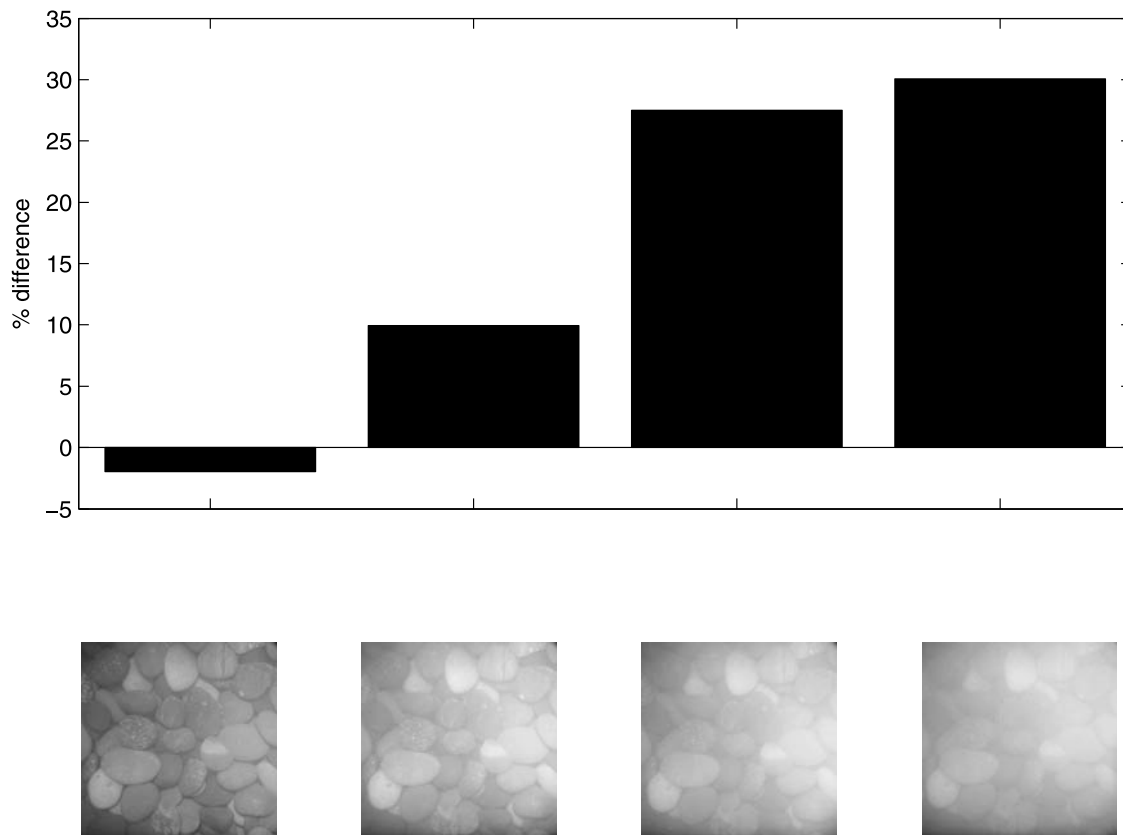


Figure 9. The effect of increasing suspended sediment concentration on size estimates of the stationary gravel bed. (top) Percent discrepancy in mean size between the point count and each estimate. (bottom) Example demeaned images (demeaning has been carried out in order to see the pebbles in the very turbid water and introduces the observed vignetting).

beds). The effect of high intragranular shading variability is to make a single grain look transitional with many smaller grains, thereby making grains appear smaller than they really are. The effect of low contrast between grains and pores is to make grains appear larger than they really are, and its effects become offset only when the intragranular shading variability increases more than eightfold. Variable intragranular shading causes variations of the order 5–10%, whereas variable intergranular shading (grain-pore contrast) causes up to 100% discrepancies between measured and estimated mean sediment size with synthetic beds. Figure 8 clearly shows that the new method is very sensitive to the relative difference between the shading of pores and grains (intergranular variation or contrast; Figure 8, right), and only weakly sensitive to intragranular (same grain) variations in shading (Figure 8, left). We conclude that the importance (to the estimated mean grain size) of high intragranular shading variability is minimal/negligible when there is low contrast between grains and pores, whereas the effect of low contrast between grains and pores is significant.

4. Effect of Variable Lighting and Suspended Sediment Concentration

[36] In order to further explore the limits of the new technique to inform its practical use, three physical experiments were carried out with photographic images of

gravel-sized sediment. The first two concern practical implementation of the new method underwater and specifically with coarse material (gravel/cobbles), for which suspended sediment concentration and refraction of light by the water/air interface will be captured in the photograph because the image must be taken at some distance above the bed through the water column. In contrast, the imaging of sand underwater is carried out close to the bed using a macro lens [e.g., Rubin *et al.*, 2007], and therefore is not affected by turbidity or random scattering of light. The third experiment concerns the photography of coarse dry sediment in direct and indirect sunlight. These experiments were just three situations out of a number of physical situations which might conceivably degrade the image for the purposes of the present technique, the full spectrum of which is somewhat beyond the scope of the present contribution. These may include shadows cast on the scene by nearby objects, small vegetation/moss etc., oblique viewing angles and image distortions (tangential, radial), the sensitivity of the new method to which would require further tests.

[37] In the first physical experiment, images were taken of well-rounded beach gravel through 50 cm of water with an inexpensive handheld waterproof camera. Point counts of the grains were carried out to calculate the true mean grain size. Increasing concentrations of mud were mixed into the water each time the bed was rephotographed. Figure 9 shows the discrepancies between true and estimated grain

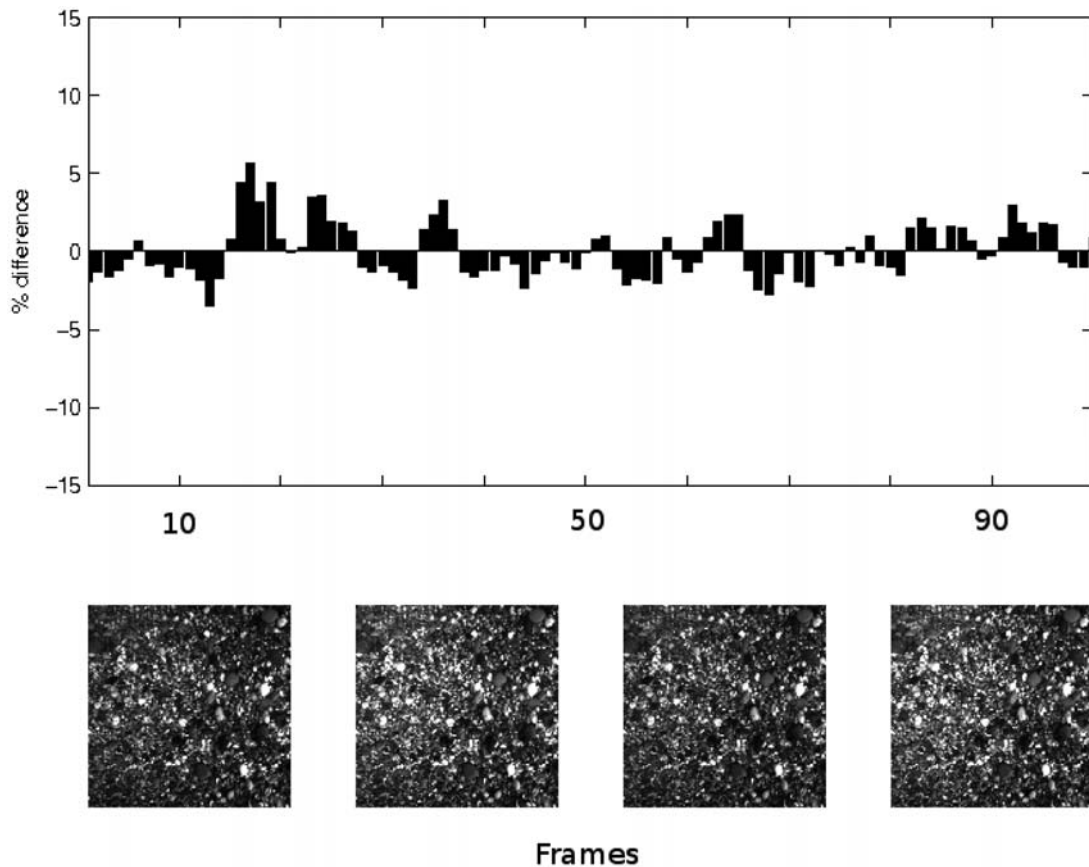


Figure 10. The effect of water waves refracting light onto a stationary gravel bed. (top) Percent discrepancy in mean size between the point count and each estimate. Frames 1, 33, 67, and 100 shown to demonstrate the range of lighting conditions.

size (in percent) with concentrations of 3.31, 5.38, and 10.31 mg/L. There is a clear and increasing positive bias in the results with increased suspended sediment concentration.

[38] The second experiment was conducted to test the effect of random ambient light by water on mean grain size estimates. One hundred images of well-rounded beach gravel were taken underwater with agitation of the water surface large enough to cause natural light to refract in random patches on the gravel surface, but small enough so as not to induce motion of the clasts. Again, point counts on one image were used as a benchmark to compare the results. Figure 10 shows the discrepancies between true and estimated mean grain size (in percent) as a result of nonuniform natural scattering of light in water. The variability was within $\pm 10\%$ which, encouragingly, is lower than the RMS error of the method.

[39] The third experiment was conducted to test the effect of variations in natural daylight, in air, on mean grain size estimates. Two images were taken of well-rounded stationary beach gravel at every hour through the day, from 1 m above the bed. The first image of each pair was unshaded, and the second shaded by an umbrella. Errors in mean grain size estimates were once again evaluated against a point count carried out on the grains in the image. Figure 11 shows the percent errors in estimates as a function of sun angle, for both the shaded (squares) and unshaded (circles) sets of photographs. Errors were of the order 15–25% when

no measures were taken to shade the grains from direct sunlight, and were minimized to within $\pm 5\%$ when images were shaded to remove large directional shadows cast by the grains on each other. These findings are consistent with the findings of *Graham et al.* [2005] and *Warrick et al.* [2009], who similarly found significant reductions in error when measures were taken to remove large shadows caused by oblique sun angles. We did not find a clear relationship between solar angle and error, however since the role of solar angle on output was not fully explored (for example at relatively high latitudes) it remains an important area of research beyond the scope of this paper. Since significant improvements occurred when lighting source was diffuse, we recommend that shading from direct sunlight is always made, because the discrepancies (in mean grain size) which may arise due to the unevenness of the surface (and possibly the intensity of sunlight) may outweigh those introduced by the angle of solar incidence.

5. Discussion

5.1. Explanation for k

[40] Mean grain size has been found to be directly related to the frequency of “typical” features in an image, a function of the wave number k which can be estimated from the image’s autocorrelogram derived by spectral means. As stated in section 2.1., the reason why k is best approximated

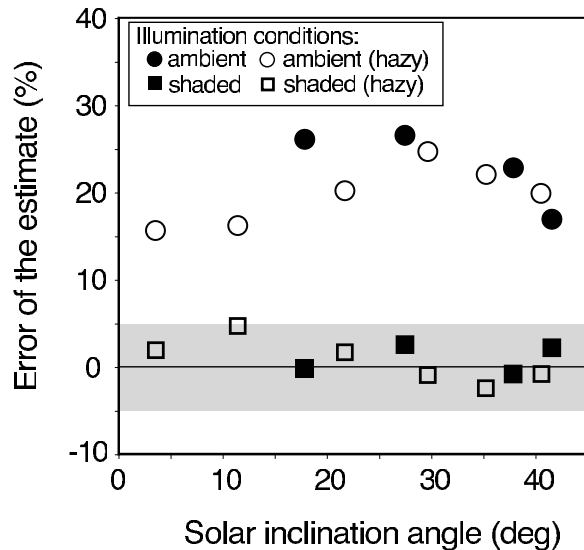


Figure 11. The effect of variable ambient solar light on size estimates of a stationary gravel bed. Percent errors are shown as a function of solar altitude angle (in degrees) for both the photographs where the grains were shaded from direct sunlight (“shaded,” corresponding to the square markers), and the photographs that were not shaded (circles). Those times where lighting conditions were hazy are denoted by filled markers.

as the lag at which the autocorrelation coefficient $R = 0.5$ is because the correlogram of a regular trigonometric series in the form e^{ikx} takes the value 0.5 at lag $\Lambda/(2\pi) = k$. Correlograms of images of sediment (and synthetic sediment surfaces) do not have this general form, however, because the features (grains) therein are not periodic, having a distribution of sizes and shapes. Instead, correlograms of sediment images are more exponential in form [Buscombe and Masselink, 2009; Warrick et al., 2009]. A more satisfactory explanation for k would therefore reconcile how a wavelength measure of a periodic function can also give the wavelength of a function with a correlogram which is exponential in form.

[41] A starting point is the idealized situation described by Rubin [2004] of a checkerboard pattern (uniform square grains shaded randomly, no overlap, and no pores), where autocorrelation at some lag less than the diameter of the “grain” depends on the fraction of offset pixels still on that same grain. In this oversimplified conceptual model, autocorrelation (given by $-0.1x + 1$, x being the spatial index, or lag) falls to 0 at the grain diameter, and at $R = 0.5$ half of the offset pixels remain in the same grain (again having a correlation of 1), and the half that shift into the next grain have a correlation of zero, combining to give 0.5. Assuming the grains are homogenous, the value $R = 0.5$ represents, statistically, the length scale over which half of the grain/pore correlations reach ≈ 0 , and half are still at ≈ 1 (on the same grain). That this is a suitable value for k is intuitively clear since it is the lag at which the data correlates half as well as at zero lag. The square grain correlogram crosses zero at lag $2k$. The correlograms of $-0.1x + 1$ and periodic function e^{ikx} pass very close to each other, and for the square grain function this occurs at $R = 0.5$ at lag $x = k$. However, real

grains in an image are not square; they have a distribution of sizes and pores separating them; and are randomly located. So we require a model for a random subdivision of space where the individual elements have a size distribution. In doing so, we can arrive at a correlogram which is exponential in form but in which k is the lag at which $R = 0.5$.

[42] Consider, then, a one-dimensional section of a binary image of grains and pores with n pixels representing pores. Assuming these n points are randomly distributed on the line of length X , the (binomial, pores being 0 and grains being 1) probability of finding exactly m ($m \leq n$) pore pixels on a line segment of length l ($x \leq X$) will be Poisson in form because n is large [Grady, 1990]; thus,

$$P(m, x) = e^{-\frac{1}{z}x} \frac{(\frac{1}{z}x)^m}{m!} \quad (5)$$

where $1/z$, or the reciprocal of mean grain size z , $\approx n/x$. The probability that there is no pore pixel on the line segment of length x (or its inverse, that there is a grain pixel on that line) is therefore given by

$$P(0, x) = e^{-\frac{1}{z}x} \quad (6)$$

which is Lineau distributed and exponential in form [Grady, 1990]. In this way, $P(0, x) = 0.5$ at z . This probability of finding pixels representing grains along a line of the same length as the mean diameter is 0.5. This is essentially the same as the well known fragmentation theory of Mott [1947], and is the case for the homogenous and isotropic sediment bed where the number of pixels representing grains and the number of pixels representing pores are equal. However, this simple model can be adjusted to account for significantly different bed sediment concentrations. Since k scales with $1/z$, the correlogram R of the function $P(0, x)$ may be given by

$$R(x) = e^{-kx} \quad (7)$$

This simple one-dimensional binary case should be valid if the image is homogenous and isotropic in geometry and shading, because all cross sections through the image will be the same in a statistical sense. In the present case, [7] can also be approximated as a function of the natural logarithm of the value of R at $x = 1$ (R_1) to give

$$R(x) = e^{ln(R_1)x} \quad (8)$$

hence packing density becomes implicit and is related to R_1 . Similar conclusions have been drawn by researchers developing stochastic models of the physical structure of porous rock [e.g., Lin, 1982; Sen, 1984; Koutsourelakis and Deodatis, 2005; Torabi et al., 2008].

[43] The gradient in the correlation surface around $R = 0.5$ gives an indication of the inherent precision in that location with respect to grain size (z). Using the simple exponential model [7] as the idealized case, we note that the slope of R will get smaller with increasing lag, so the slope at lag associated with $R = 0.5$ will always take on intermediate values. We also note that the slope of R at this point will diminish with increasing k . The sensitivities of R to changes in, respectively, k or x may be assessed using the derivatives

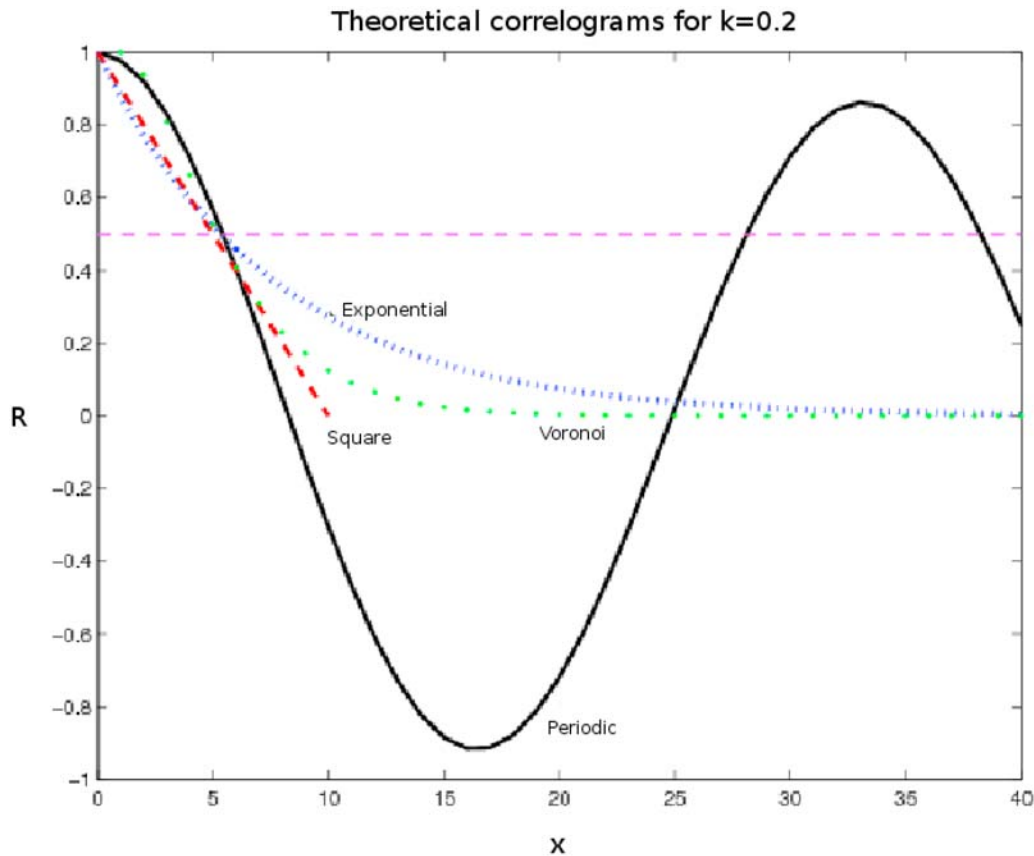


Figure 12. Theoretical correlograms for the square grain idealized case (*Rubin* [2004]; red dashed line) as a function of lag x ; a periodic function (black solid line); an exponential function (equation (7), blue dotted line), and a Poisson-Voronoi tessellation (equation (11), green dots), all with “typical feature length” $k = 5^{-1}$. The exponential curve has been constructed using bed packing concentration $c = 0.65$. Note how the exponential, Poisson, and periodic correlograms equal 0.5 (horizontal dashed line) at identical lag.

of [7] which are given by $dR/dx = -ke^{-xk}$ and $dR/dk = -xe^{-xk}$. Of most relevance are the changes in R as a function of changes in x which are, using [4], given by $(-1/\pi)k$ (but due to discretization into 1 pixel steps an approximation $-k^{1/3}$ should suffice). One pixel step is equivalent to $(2\pi)dz$ or $e^{-dk} - 1$. This is a first approximation on the typical sensitivities. Since this will be affected primarily by anisotropy in the 2D correlogram, and variable sediment sorting, more precision would be achieved empirically.

[44] The simplicity of the stochastic geometric model of equation (7) allows its relationship to the spectral theory of section 2.1 to be formalized as follows. Substituting $P(z)$ for $P(x)$, the characteristic function $\phi(k)$ may be defined as the Fourier transform (Γ) of the probability density function [*Brown and Hwang*, 1997], which here is defined

$$\phi(k) = \Gamma[P(z)](k) = \int_{-\infty}^{\infty} e^{ikz} f(z) dz \quad (9)$$

Since the total integral of $P(z)$ is 1 ($\int_{-\infty}^{\infty} \phi(k) dz$), the probability density can be recovered using an inverse Fourier transform:

$$P(z) = \Gamma_k^{-1}[\phi(k)](z) = \frac{1}{2\pi} \int_{-\infty}^{\infty} e^{-ikz} \phi(k) dz \quad (10)$$

[45] We also note that the Poisson-Voronoi tessellations used as the basis for the computer simulations in section 3 would be entirely consistent with the earlier observation that particles are distributed according to the theory of *Mott* [1947], since fragmented (fractured) surfaces also consist of convex polygons [*Grady*, 1990]. It is also important to note that curves generated by the cumulative probability density function of a Poisson-Voronoi tessellation, as given by *Muche and Stoyan*, [1992], and in the same notation as equation (7), would give a correlogram in the form:

$$R(x) = (1 + 2kx)e^{-2kx} \quad (11)$$

[46] Figure 12 summarizes how the spectral k of section 2.1, from a periodic function, is useful in describing the exponential correlograms of real sediment. The lag at which the correlogram of the periodic function e^{-ikx} has the value 0.5 is also the same lag at which the exponential correlogram (equation (7)) has the value 0.5. Note that $R(x) = e^{-kx}$ reaches 0, and e^{-ikx} completes one cycle, at $\Lambda = (2\pi)/k$. The theoretical correlogram of a Poisson-Voronoi tessellation (equation (11)) also passes very close to 0.5 at lag k , which explains its usefulness in modeling natural sediment beds.

The key information content of the image with respect to mean grain size is therefore in the high frequency part of the correlogram (and spectrum) up to $R = 0.5$. The divergence of the correlograms after that point is irrelevant to the calculation of mean grain size. However, for estimation of the entire grain size distribution there is likely to be the most information content where the correlogram has the greatest curvature. We have presented three new possible models of a sediment image correlogram which may be a starting point for research into estimation of more parameters of interest from photographs of natural beds, including the distribution of sizes.

5.2. Note on Image Resolution

[47] The minimum resolvable grain size is a function of spatial resolution and area of the image, and the distribution of grain sizes. While it is often possible to tell by eye if grains in the image are resolved, it would be more useful if quality control was achieved through the use of an automated and quantitative measure of how resolved the grains are. Therefore, experiments were conducted in order to find an objective measure of image resolution with respect to the features within. The approach taken was to progressively downsample images (i.e., interpolate over a smaller grid) of synthetic and real sediment. It was determined empirically that a suitable definition for an underresolved image, ascertained subjectively by eye and also objectively as the point which sees the greatest decrease in standard deviation per unit downsample rate, is one whose autocorrelation value at lag 1 is $\leq \sqrt{1/2} \approx 0.7$. The theoretical autocorrelation curve where $R(1) = \sqrt{1/2}$, as expressed by equation (8), may be taken as an approximation to the correlogram at the threshold between adequately and not adequately resolved. This yields a minimum grain radius of 2–3 pixels, which seems reasonable both intuitively and visually, and also agrees with the minimum workable grain scale of *Warrick et al.* [2009].

[48] The value $R = 0.5$ always corresponds to the most linear and steepest part of the correlogram of an image. Since grain size and lag are related by two scalars (2π and r), the same applies when the correlogram is expressed in physical units of length rather than pixels. While ellipse fitting (Appendix A) can return typical lag k at subpixel precision (i.e., decimal lags), sensitivities in grain size are potentially high to small deviations away from $R = 0.5$ in this region (e.g., 0.49 or 0.51: section 5.1 discusses the sensitivities using the derivatives of (4)). The effect could be introducing error to the estimated mean grain sizes and while beyond the scope of the present contribution to quantify this experimentally, we predict that in practice this is only a concern when the image resolution is relatively poor, near the limit of 2–3 pixels suggested above.

5.3. Summary and Recommendations

[49] The new method reads grain size directly from the image, and produces a result which is most closely related to the mean intermediate (b axis) particle diameter. This measure has been found to be a linear function of the radius of an ellipse fitted to the $R = 0.5$ contour of the 2D autocorrelogram (according to the method in Appendix A). This radius may be thought of as the mean section length from edge to center of the ellipse. No averaging takes place in the

estimate, over individual particles or sediment size classes. The measure may be thought of as more closely related to the mean of individual particle diameters rather than the moment-derived mean of a size distribution evaluated over discrete grain size classes. The measure of sediment size against which estimates have been compared is the mean of 100 particles, randomly sampled, on corresponding images, measured by eye from pore to pore across the intermediate (b) axis of the particle (here called point counts). The method presented here is sensitive to the major axes of the projected areas of grains lying imperfectly in a semiplane, which has been shown by *Kellerhals et al.* [1975] to, given sufficient sample size, satisfactorily approximate the true mean intermediate (b) axis. Thus our method inherently accounts for the effects of overlapping grains. A correction factor would have to be applied to the results of the technique outlined in this contribution in order to provide estimates of the mean long (a) and short (c) axes of particles.

[50] A number of recommendations can be made with the general use of the new method. For example, correlograms with value at lag 1 $\leq \sqrt{1/2} \approx 0.7$ should be removed because it is likely that the grains are underresolved. Autocorrelation should be calculated over sufficient lags to ensure R falls to below 0.5. However, there is no new information related to mean grain size at lags beyond that at which $R = 0$. Since there is a disproportionate amount of information in the first few lags, autocorrelation should be calculated for every 1 pixel shift (unless, conceivably, image resolution is unusually high in which case there is little new information at each pixel lag). Lighting of sediment should be optimized so the contrast between pores and grains is maximized without overexposing either and avoiding strong reflections from grain facets and crystal faces. Collectively, this means lighting as diffuse as possible with no gradient perceivable by eye, which further means that lighting from at least two opposing sides of the image rather than above should find greater success.

[51] Computer simulations highlighted the sensitivities of the measure to the relative difference between the shading of pores and grains (intergranular shading), and only weakly sensitive to intragranular (same grain) variations in shading/color. The contrast between grains and pores (the intergranular spaces) should be maximized and, in an adequately resolved image, appears more important than intragranular (same grain) shading. This factor should be considered in the design of lighting for the photograph collection. The measure is sensitive to anything which obscures the variation in intensity at the grain scale, which includes large distortions in the image. These macroscale variabilities are in general more important to grain size errors than microscale variabilities, i.e., subgrain and subpixel [cf. *Carbonneau*, 2005].

[52] Physical experiments showed that turbid water caused significant discrepancies (up to 40%) between estimated and measured grain size, but that random refraction of light caused by water waves did not create a larger error (within $\pm 10\%$) than the inherent error in the method. Errors were minimized to within $\pm 5\%$ in images of gravel beds in air, illuminated by ambient solar light, when images were shaded to remove large directional shadows cast by the grains on each other.

[53] The insights obtained here may also be used to optimize the use of spatial autocorrelation technique of

Rubin [2004], which solves for mean grain size using a least squares fit between the correlogram of a sample image (of unknown mean grain size) and a catalogue of correlograms associated with sediment of known mean grain size. For example, the theoretical forms of the correlogram as presented in this paper may be of use in the selection of grain size fraction spacing, and other ways pertinent to calibration catalogue design. We also note that equation (4) should have a similar derivation for other similar statistical approaches, for example semivariance [e.g., *Carbonneau et al.*, 2004, 2005; *Verdú et al.*, 2005; *Buscombe and Masselink*, 2009].

[54] There may be a unique value of R associated with several percentiles of the grain size distribution, but this may be restricted to idealized cases of very well sorted sediment photographed at very high resolution. The highest level of precision will be achieved if the new method is partially calibrated. By this we mean that, if point counts on (fine and coarse) end-members of individual sediment populations reveal significant bias (in the form of an apparent slope in data away from the 1:1 line, e.g., Figure 4), maximum precision will be achieved by carrying out a reduced major axis regression and correcting for the slope of the bias.

6. Conclusions

[55] A new method for characterizing mean grain size has been proposed, utilizing the spectral properties of an image of sediment. It is designed to provide a robust approximation to mean grain size from any image of noncohesive sediment taken under controlled conditions. Like other image-based methods, it is inexpensive, rapid and unintrusive.

[56] It has been shown to work well for sand, gravel and cobble-sized sediment, providing an estimate of mean grain size with an RMS error of $\sim 16\%$, and with a 95% probability of estimates within 31% of the true mean grain size without any calibration. It is thus fully transferable between all noncohesive sediment types. The RMS error reduced to $\sim 11\%$, with a 95% probability of estimates within 20% of the true mean grain size if point counts from a few images are used to correct the bias for a specific population of sediment images. A combination of theory, computational experiments, and physical experiments was used to both understand and explore the sensitivities and limits of this new method.

[57] Like previous statistical approaches, the method described in this contribution has circumnavigated the difficult problem of detecting individual grains in a rigorous way which is portable across different size fractions. Unlike previous statistical methods, however, calibration is not required for individual sedimentary environments. Collectively, this has allowed the development of a fully transferable method for the first time. In addition, the stochastic approach has facilitated the expression of the spatial distribution of pixel intensity within the image of sediment to the mean grain size in a mathematical way.

[58] The adoption of a statistical approach to mean grain size estimation from images of sediment avoids the complexities of a deterministic approach for application to noncohesive sediment of all sizes, mineralogies, and types. The spectrum of an image is an ideal tool to detect the mean length scale of intensity variation because it receives contributions from all spatial frequencies and orientations

simultaneously. The method is computationally efficient (an image of several megapixels in size may be processed in just a few seconds), and does not require identification and measurement of any individual grains. Indeed, in the approach outlined here the distribution is not required for estimating the mean grain size. Hence, there are fewer sensitivities to the tails of the population, and no truncation is necessary. However, further work should uncover statistical measures derived directly from the two-dimensional autocorrelogram which are sensitive to percentiles of the grain size distribution, from which other sedimentological parameters such as sorting, or other properties of interest, might be derived. The new method described here may also be useful for quantifying the dominant wavelength of other suitably homogenous entities within images.

Appendix A: Ellipse Fitting to Contour $R = 0.5$

[59] An ellipse is fitted to a contour described by the coordinates $[m, n]$ using a second-order polynomial given by

$$F(m, n) = am^2 + bmn + cn^2 + dm + en + f = 0 \quad (\text{A1})$$

where $\mathbf{a} = [a, b, c, d, e, f]^T$ are coefficients, and T denotes transpose. We use the least squares method of *Fitzgibbon et al.* [1999], as detailed in the work of *Buscombe* [2008]. Where \Im denotes imaginary part and N is the number of coordinate pairs, the mean ellipse radius (lags in units of pixels) is found as

$$k = \frac{\sum \Im(\sqrt{0 - m^2 + 0 - n^2})}{N} \quad (\text{A2})$$

[60] It is, however, more likely that the contour is non-circular and thus k may vary as a function of cross section through the autocorrelation surface (if the grains or other features such as light speckles in the image have any preferred orientation). The ellipse can be sectioned in infinite planes, and each will give a slightly different result. We determined that the value of k which most closely corresponds to the mean of the intermediate axes of the grains is the radius of the ellipse given by

$$k = 1/\sqrt{\zeta v} \quad (\text{A3})$$

where $\zeta = 1/(\epsilon^T E \times \epsilon - f)$, using translations given by:

$$E = [a, b/2]^T [b/2, c]^T \quad (\text{A4})$$

and

$$\epsilon = -(2E)^{-1} [d, e]^T \quad (\text{A5})$$

and where $s_1 = \cos(\theta)$; $s_2 = \sin(\theta)$; and θ is the ellipse orientation:

$$v = (as_1s_2) - (bs_1s_2) + (cs_1^2) \quad (\text{A6})$$

Appendix B: Maximum Likelihood Estimate of Log-Hyperbolic Probability Density Function

[61] The log-hyperbolic distribution is a four-parameter $(\alpha, \beta, \delta, \mu)$ density function. The maximum likelihood estimates of the parameters are found by iteratively minimizing the density function using all four parameters simultaneously. Here, the approach taken was to minimize the density function of the hyperbolic distribution in the following form, with respect to the Lebesgue measure [Jensen, 1988]

$$\frac{\sqrt{\alpha^2 - \beta^2}}{2\delta\alpha K\left(\delta\sqrt{\alpha^2 - \beta^2}\right)} e^{-\alpha\sqrt{\delta^2 + (x-\mu)^2} + \beta(x-\mu)} \quad (\text{B1})$$

where $\alpha > 0$, $\alpha > \|\beta\|$ and $\delta > 0$, subject to $\int p(x) = 1$, using the unconstrained nonlinear optimization derivative-free simplex method of Lagarias *et al.* [1998] which can handle discontinuities, for example when $\delta = 0$ [see Fieller *et al.*, 1992]. The modified Bessel function K was of the 2nd kind, and its constant set to unity. For a more detailed description of the parameters refer to Barndorff-Nielsen [1977] and Fieller *et al.* [1992]. For a review on the computational aspects of hyperbolic distribution fitting the reader is referred to McArthur [1986] and Jensen [1988].

[62] **Acknowledgments.** Thanks to Parker Allwardt, Sarah McNaboe, Melinda Garvey, and Liron Friedman for carrying out manual point counts on images. Thanks to Patrick Barnard, Katie Farnsworth, Andrew Stevens, and Doug George for collecting several sediment images. Hank Chezar, Gerry Hatcher, and Rob Wyland helped with the design and fabrication of the camera systems. Many images were collected on projects funded by the USGS, Glen Canyon Adaptive Management Program, and Office of Naval Research. The manuscript benefited from reviews by Matthew Arsenault, Scott Wright, Patrice Carbonneau, and two anonymous reviewers. Special thanks to the Editor for his helpful suggestions regarding the calculation and presentation of our errors. A program (My Automated Grain size from Images Code - MAGIC) written in both MATLAB® and Python is available from the authors. The use of MATLAB® trade name is for descriptive purposes and does not constitute endorsement by the USGS.

References

- Bader, H. (1970), Hyperbolic distribution of particle sizes, *J. Geophys. Res.*, *75*, 2822–2830.
- Barnard, P. L., D. M. Rubin, J. Harney, and N. Mustain (2007), Field test comparison of an autocorrelation technique for determining grain size using a digital ‘beachball’ camera versus traditional methods, *Sediment. Geol.*, *201*, 180–195.
- Barndorff-Nielsen, O. (1977), Exponentially decreasing distributions for the logarithm of particle size, *Proc. R. Soc. London A*, *353*, 401–419.
- Barndorff-Nielsen, O. (1989), Sorting, texture and structure, *Proc. R. Soc. Edinburgh*, *96B*, 167–179.
- Brown, R. G., and P. Y. C. Hwang (1997), *Introduction to Random Signals and Applied Kalman Filtering*, 484 pp., John Wiley, New York.
- Buscombe, D. (2008), Estimation of grain-size distributions and associated parameters from digital images of sediment, *Sediment. Geol.*, *210*, 1–10.
- Buscombe, D., and G. Masselink (2009), Grain size information from the statistical properties of digital images of sediment, *Sedimentology*, *56*, 421–438.
- Buscombe, D., G. Masselink, and D. M. Rubin (2008), Granular properties from digital images of sediment: Implications for coastal sediment transport modelling, in *Coastal Engineering 2008: Proceedings of the 31st International Conference on Coastal Engineering*, vol. 2, edited by J. M. Smith, pp. 1625–1637, World Sci., London.
- Carbonneau, P. E. (2005), The threshold effect of image resolution on image-based automated grain size mapping in fluvial environments, *Earth Surf. Processes Landforms*, *30*, 1687–1693.
- Carbonneau, P. E., S. N. Lane, and N. Bergeron (2004), Catchment scale mapping of surface grain size in gravel bed rivers using airborne digital imagery, *Water Resour. Res.*, *40*, W07202, doi:10.1029/2003WR002759.
- Carbonneau, P. E., N. Bergeron, and S. N. Lane (2005), Automated grain size measurements from airborne remote sensing for long profile measurements of fluvial grain sizes, *Water Resour. Res.*, *41*, W11426, doi:10.1029/2005WR003994.
- Davis, J. C. (1986), *Statistics and Data Analysis in Geology*, (2nd ed.), 646 pp., John Wiley, New York.
- Fara, H. D., and A. E. Scheidegger (1961), Statistical geometry of porous media, *J. Geophys. Res.*, *66*, 3279–3284.
- Fieller, N. R. J., E. C. Flenley, and W. Olbricht (1992), Statistics of particle-size data, *Appl. Stat.*, *41*, 127–146.
- Fitzgibbon, A. W., M. Pilu, and R. B. Fisher (1999), Direct least square fitting of ellipses, *IEEE Trans. Pattern Anal. Mach. Intel.*, *21*, 476–480.
- Folk, R. L., and W. C. Ward (1957), Brazos River bar: A study in the significance of grain size parameters, *J. Sediment. Petrol.*, *27*, 3–26.
- Grady, D. E. (1990), Particle size statistics in dynamic fragmentation, *J. Appl. Phys.*, *68*, 6099–6105.
- Graham, D. J., S. P. Rice, and I. Reid (2005), A transferable method for the automated grain sizing of river gravels, *Water Resour. Res.*, *41*, W07020, doi:10.1029/2004WR003868.
- Griffiths, J. C. (1961), Measurement and properties of sediments, *J. Geol.*, *69*, 487–498.
- Jensen, J. L. (1988), Maximum-likelihood estimation of the log-hyperbolic parameters from grouped observations, *Comput. Geosci.*, *14*, 389–408.
- Kellerhals, R., J. Shaw, and V. K. Arora (1975), On grain size from thin sections, *J. Geol.*, *83*, 79–96.
- Koutsourelakis, P. S., and G. Deodatis (2005), Simulation of binary random fields with applications to two-phase random media, *J. Eng. Mech.*, *131*, 397–412.
- Lagarias, J. C., J. A. Reeds, M. H. Wright, and P. E. Wright (1998), Convergence properties of the Nelder-Mead simplex method in low dimensions, *SIAM J. Optim.*, *9*, 112–147.
- Lian, T. L., P. Radhakrishnan, and B. S. D. Sagar (2004), Morphological decomposition of sandstone pore-space: Fractal power-laws, *Chaos, Solitons Fractals*, *19*, 339–346.
- Lin, C. (1982), Microgeometry I: Autocorrelation and rock microstructure, *Math. Geol.*, *14*, 343–360.
- McArdle, B. H. (1988), The structural relationship: regression in biology, *Can. J. Zool.*, *66*, 2329–2339.
- McArthur, D. S. (1986), Derivatives and FORTRAN subroutines for a least-squares analysis of the hyperbolic distribution, *Math. Geol.*, *18*, 441–450.
- Mott, N. F. (1947), Fragmentation of shell cases, *Proc. R. Soc. London A*, *189*, 300–308.
- Muche, L., and D. Stoyan (1992), Contact and chord distributions of the Poisson-Voronoi tessellation, *J. Appl. Probab.*, *29*, 467–471.
- Preston, F. W., and J. C. Davis (1976), Sedimentary porous materials as a realization of a stochastic process, in *Random Processes in Geology*, edited by D. F. Merriam, pp. 63–86, Springer, New York.
- Rice, S., and M. Church (1996), Sampling surficial fluvial gravels: The precision of size distribution percentile estimates, *J. Sediment. Res.*, *66*, 654–665.
- Rubin, D. M. (2004), A simple autocorrelation algorithm for determining grain size from digital images of sediment, *J. Sediment. Res.*, *74*, 160–165.
- Rubin, D. M., H. Chezar, J. N. Harney, D. J. Topping, T. S. Melis, and C. R. Sherwood (2007), Underwater microscope for measuring spatial and temporal changes in bed-sediment grain size, *Sediment. Geol.*, *202*, 402–408.
- Sen, Z. (1984), Autorun analysis of sedimentary porous materials, *Math. Geol.*, *16*, 449–463.
- Sime, L. C., and R. I. Ferguson (2003), Information on grain sizes in gravel-bed rivers by automated image analysis, *J. Sediment. Res.*, *73*, 630–636.
- Torabi, A., H. Fossen, and B. Alaei (2008), Application of spatial correlation functions in permeability estimation of deformation bands in porous rocks, *J. Geophys. Res.*, *113*, B08208, doi:10.1029/2007JB005455.
- Tovey, N. K., and M. W. Hounslow (1995), Quantitative micro-porosity and orientation analysis in soils and sediments, *J. Geol. Soc. London*, *152*, 119–129.
- Verdú, J. M., R. J. Batalla, and J. A. Martínez-Casanovas (2005), High-resolution grain-size characterisation of gravel bars using imagery analysis and geo-statistics, *Geomorphology*, *72*, 73–93.
- Warrick, J. A., D. M. Rubin, P. Ruggiero, J. Harney, A. E. Draut, and D. Buscombe (2009), Cobble Cam: Grain-size measurements of sand to boulder from digital photographs and autocorrelation analyses, *Earth Surf. Processes Landforms*, *34*, 1811–1821.

D. Buscombe, School of Marine Science and Engineering, University of Plymouth, Plymouth PL4 8AA, UK. (daniel.buscombe@plymouth.ac.uk)
 D. M. Rubin and J. A. Warrick, U.S. Geological Survey, Santa Cruz, CA 95060, USA. (drubin@usgs.gov; jwarrick@usgs.gov)